# Molecular origins of nonlinear optical activity in zinc tris(thiourea)sulfate revealed by high-resolution x-ray diffraction data and *ab initio* calculations

Jacqueline M. Cole[1,2,*] and Daniel D. Hickstein[1]

[1]*Cavendish Laboratory, University of Cambridge, J. J. Thomson Avenue, Cambridge CB3 0HE, United Kingdom*

[2]*Department of Physics and Department of Chemistry, University of New Brunswick, P.O. Box 4400, Fredericton, Canada E3B 5A3*

(Received 9 September 2012; published 18 November 2013)

Structure-property relationships are established in the nonlinear optical (NLO) material, zinc tris(thiourea)sulfate (ZTS), via an experimental charge-density study, x-ray constrained wave-function refinement, and quantum-mechanical calculations. The molecular charge-transfer characteristics of ZTS, that are important for NLO activity, are topologically analyzed via a multipolar refinement of high-resolution x-ray diffraction data, which is supported by neutron diffraction measurements. The extent to which each chemical bond is ionic or covalent in nature is categorized by Laplacian-based bonding classifiers of the electron density; these include bond ellipticities, energy densities, and the local source function. Correspondingly, the NLO origins of ZTS are judged to best resemble those of organic NLO materials. The molecular dipole moment, $\boldsymbol{\mu_i}$, and (hyper)polarizability coefficients, $\boldsymbol{\alpha_{ij}}$ and $\boldsymbol{\beta_{ijk}}$, are calculated from the experimental diffraction data using the x-ray constrained wave-function method. Complementary gas-phase *ab initio* quantum-mechanical calculations of $\boldsymbol{\mu_i}$, $\boldsymbol{\alpha_{ij}}$, and $\boldsymbol{\beta_{ijk}}$ offer a supporting comparison. When taken alone, the experimental charge-density analysis does not fare well in deriving $\boldsymbol{\mu_i}$, $\boldsymbol{\alpha_{ij}}$, or $\boldsymbol{\beta_{ijk}}$, which is not entirely surprising given that the associated calculations are only generally valid for organic molecules. However, by refining the x-ray data within the constrained wave-function method, the evaluations of $\boldsymbol{\mu_i}$, $\boldsymbol{\alpha_{ij}}$, and $\boldsymbol{\beta_{ijk}}$ are shown to agree very well with those from *ab initio* calculations and show remarkable normalization to experimental refractive index measurements. The small differences observed between *ab initio* and x-ray constrained wave-function refinement results can be related directly to gas- versus solid-state phase differences. $\boldsymbol{\mu_i}$ is found to be 28.3 Debye (gas phase) and 29.7 Debye (solid state) while $\boldsymbol{\beta_{ijk}}$ coefficients are not only significant but are also markedly three dimensional in form. Accordingly, substantial octupolar as well as dipolar NLO contributions in ZTS are indicated, which challenges the traditional focus on dipolar NLO molecules. This evaluation of NLO properties and their relation to the molecular structure offers several ways by which ZTS may be more widely functionalized as a NLO material. More generally, this case study on ZTS demonstrates how experimental and computational techniques can be combined to understand NLO structure-property relationships, an important tool for the quantum-tailored molecular design of next-generation metalorganic NLO materials.

DOI: 10.1103/PhysRevB.88.184105 PACS number(s): 61.50.Ah, 42.65.An, 61.05.cp

## I. INTRODUCTION

Metalorganic compounds present a largely unexplored area of materials discovery for nonlinear optical (NLO) applications. This is likely to be due to the far more complicated structure-property relationships that govern metalorganic NLO activity compared with organic materials,[1,2] and yet, their potential is staggering. They possess all of the inherent strengths of organic materials compared with inorganics (faster optical response times, significantly higher optical outputs, and much greater versatility in molecular design) while maintaining the primary assets of inorganic NLO materials (good thermal stability and high laser damage thresholds). Their potential goes well beyond this ideal inorganic-organic "compromise." For instance, their high-coordinate geometry, with the electron donor (metal) at the center of the molecular symmetry, affords a perfect topology for exploitation as octupolar NLO materials. Tetrahedral, square planar, and octahedral metal coordination geometries are very pertinent in this regard.[2–5]

Despite all of these intrinsic advantages of metalorganic compounds for NLO applications, the field remains largely untapped. Zinc tris(thiourea)sulfate (hereafter ZTS; Fig. 1) is one of the few metalorganic NLO materials that has been tested seriously for industrial potential. In addition to being air stable (owing to the complete 3*d* electronic configuration of Zn), ZTS also bears a strong relation to urea—the classic reference material for second-harmonic generation (SHG). It was therefore natural to consider urea and its close chemical relatives as ligands when first exploring the NLO prospects of metalorganic coordination complexes. Several promising candidates resulted from these exploratory studies.[6–9] ZTS was deemed the most promising on account of its plethora of electro-optic, piezoelectric, dielectic,[10] nonlinear optical,[9] and thermal properties.[11] Specifically, ZTS demonstrated an SHG output that is comparable to that of potassium dihydrogen phosphate (KDP). ZTS also displays a very low power threshold for observable SHG, it is critically phase matchable, it has a heat capacity and thermal expansivity which varies linearly with temperature, and a large thermal conductivity anisotropy (conductivity along the crystallographic direction, $c \gg a$). The optical properties of deuterated ZTS are similarly appealing, although the SHG behavior is not phase matchable.[12]

Spectroscopic[13] and crystallographic[14–17] materials characterization has also been carried out on ZTS. While such studies represent an important contribution to realizing the potential of ZTS, a detailed investigation of the structure-property relationships on ZTS remains untold; yet this is needed in order to more fully assess the potential of ZTS as an NLO material.

 

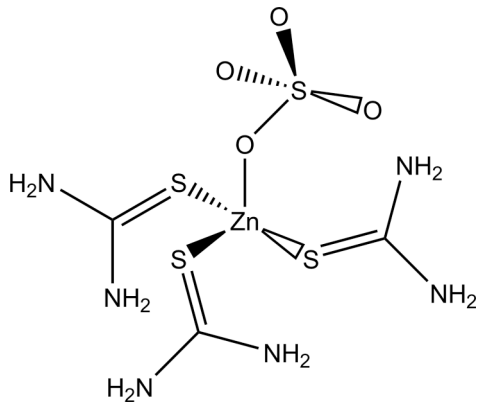


FIG. 1. Chemical schematic diagram of the zinc tris(thiourea)sulfate (ZTS) molecule.

Furthermore, while the structural origins of second-order NLO activity in organic and inorganic materials are well understood, metalorganics are effectively a "hybrid" of these two material types and the structural origins of the NLO behavior are not fully understood. The structure-property relationships thus generated in ZTS can then help stimulate and foster the molecular engineering of other metalorganic materials.

Conventional x-ray diffraction experiments using the independent atomic model (IAM) are not suited to the task of rationalizing the structure-property relationships of NLO materials. This is because the IAM does not distinguish bonding density and assumes no atomic charges. Yet, such discrimination is critical in a detailed analysis of highly polarizable molecules, such as NLO compounds, where the key information lies within the valence electron density of a delocalized-charge structure, owing to prevailing charge-transfer effects. Therefore, one must turn to a much more sophisticated approach of structural enquiry.

In this study, we use charge-density crystallography techniques to model the complete electron density of ZTS. This employs high-resolution x-ray diffraction data embedded within a multipolar formalism.[18] This models electron density around atoms using spherical harmonics and Slater-type radial functions; the implicit relationship between spherical harmonics and bond orbital topologies thereby takes into account bonding density explicitly. A charge-density study can therefore refine electron distributions, partitioning them into distinct orbital representations. Such partitioning also enables the calculation of atomic charges.

The multipolar refinement permits a topological analysis of the valence bonding orbitals throughout the molecule, enabling a quantitative examination of the nature of bonding and a determination of electronic charge-transfer characteristics that underpin the structural origins of an NLO material;[4] cf. the polarization response to an electric field that defines NLO phenomena at the molecular level according to the power series

$$\mathbf{P_i} = \boldsymbol{\mu}_\mathbf{i} + \boldsymbol{\alpha}_\mathbf{ij}\mathbf{E_i} + \boldsymbol{\beta}_\mathbf{ijk}\mathbf{E_i}\mathbf{E_j} + \boldsymbol{\gamma}_\mathbf{ijkl}\mathbf{E_i}\mathbf{E_j}\mathbf{E_k} + \cdots, \quad (1)$$

where $\mathbf{P_i}$ is the electronic polarization of a molecule subject to an electric field $\mathbf{E}$, $\boldsymbol{\mu}_\mathbf{i}$ is the dipole moment of the molecule, $\boldsymbol{\alpha}_\mathbf{ij}$ is the molecular polarizability, $\boldsymbol{\beta}_\mathbf{ijk}$ is the first molecular hyperpolarizability, $\boldsymbol{\gamma}_\mathbf{ijkl}$ is the second molecular hyperpolarizability, and so on. The first nonlinear term ($\boldsymbol{\beta}_\mathbf{ijk}$) corresponds to the intrinsic ability of a molecule to exhibit SHG; it is a third-rank tensor and so its projection can be described by 27 independent terms. By extension, the successive nonlinear terms ($\boldsymbol{\gamma}_\mathbf{ijkl}$ and so on) represent third-, fourth-, . . . harmonic generation and are fourth-, fifth-, . . . rank tensors.

The paper then proceeds to consider possible ways to derive the associated electronic polarization terms from this charge-density study. In principle, the atomic partitioning of multipolar moments from molecular charge-density topologies can be undertaken, and used to calculate the full set of tensorial components $\boldsymbol{\beta}_\mathbf{ijk}$ (as well as $\boldsymbol{\mu}_\mathbf{i}$ and $\boldsymbol{\alpha}_\mathbf{ij}$) in the solid state.[19] However, the calculation of $\boldsymbol{\beta}_\mathbf{ijk}$ requires a few *a priori* assumptions, one of which is that the compound is a relatively homogeneous molecule, i.e., it comprises elements of similar numbers of electrons (e.g., an organic molecule). The validity of this assumption for ZTS is somewhat tenuous, given its elemental makeup. Nevertheless, an attempt is herein made to evaluate $\boldsymbol{\beta}_\mathbf{ijk}$ via the charge-density study. While we show that this does not fare well on its own account, the calculation of these coefficients from a refined structural model that uses the x-ray constrained wave-function method[20] is found to produce very reliable results.

The x-ray constrained wave-function method can be thought of as a hybrid of computation and experiment. Therein, the experimental atomic coordinates from the multipolar refinement are first used to compute a wave function of a molecule of ZTS within a noninteracting environment. Theoretical x-ray structure factors are then generated from this wave function which are subsequently refined against the experimental structure factors taken from the charge-density study. We show that calculations of $\boldsymbol{\mu}_\mathbf{i}$, $\boldsymbol{\alpha}_\mathbf{ij}$, and $\boldsymbol{\beta}_\mathbf{ijk}$ from x-ray constrained wave-function refinements compare very well to supporting *ab initio* calculations, and to baseline refractive index measurements.

The results of these calculations enable an assessment of the extent to which the molecular symmetry of ZTS conforms to octupolar symmetry requirements. The ZTS molecule possesses pseudo-threefold symmetry that approximates molecular point group $C_3$. This is one of the defining point-group symmetries for delivering an octupolar $\boldsymbol{\beta}_\mathbf{ijk}$ response.[1] Octupolar materials present a very attractive prospect since they afford a nonlinear optical response over a wide range of three-dimensional space. Contrast this with the historical restrictive exploration on dipolar materials which has optimized $\boldsymbol{\beta}_\mathbf{ijk}$ predominantly in one dimension.[21] The identification and quantification of octupolar characteristics in nonlinear optical materials can therefore be assessed by comparing the $\boldsymbol{\beta}_\mathbf{ijk}$ tensorial components in terms of a two- versus three-dimensional level of contribution. The consideration of octupolar NLO contributions in materials is a worthy goal since it not only stands to gain geometric spread of the first molecular hyperpolarizability but it could also augment its overall NLO output.

## II. EXPERIMENTAL AND METHOD DETAILS

### A. High-resolution x-ray diffraction data

A $0.20 \times 0.15 \times 0.10$ mm$^3$ single crystal of ZTS was grown by slow evaporation from aqueous solution.[22] This was mounted onto a Bruker SMART charge-coupled device (CCD)

diffractometer, equipped with graphite monochromated Mo $K\alpha$ x-ray radiation ($\lambda = 0.710\,73$ Å). An Oxford Cryosystems open-flow nitrogen Cryostream cooled and maintained the sample at 100 K. High-resolution x-ray diffraction images were collected, yielding 13 998 usable reflections out to a $\sin\theta/\lambda$ of 1.10 Å$^{-1}$. The SMART software suite[23] was employed for all cell refinement and data collection procedures, while the SAINT integration programs[24] were used for data reduction. An absorption correction was performed using SORTAV (Ref. 25) and merged using DREAM.[26] A conventional independent atom model (IAM) structure determination, using SHELX97 and SHELXTL,[27] confirmed the space group $Pca2_1$ (with $a =$ 11.0673 Å; $b = 7.7342$ Å; $c = 15.5573$ Å; $Z = 4$) and the absolute structure of ZTS with the refined Flack parameter,[28] $-0.0012(21)$. Positional and anisotropic displacement parameters (ADPs) for all nonhydrogen atoms were refined by full-matrix least-squares refinement. Hydrogen atoms were positioned with idealized geometries and their ADPs constrained according to the riding model, $U_{eq}(H) = 1.2U_{eq}(C)$.

### B. Multipolar refinement

Initial atomic coordinates and anisotropic displacement parameters for the multipolar refinement were taken from the IAM refinement of the x-ray data in the case of all nonhydrogen atoms. Those for hydrogen atoms were imported directly from a 100 K neutron diffraction study on ZTS (Ref. 15) and were fixed in all subsequent refinements. The multipolar refinement was enabled via the XD2006 suite of programs.[29] Full details are given in the Supplemental Material.[30]

Residual electron-density maps of the final charge-density model of ZTS (see Supplemental Material[30]) were essentially featureless at the 0.1 $e$ Å$^{-3}$ level with the exception of the areas around S and Zn. Here, up to 0.2 $e$ Å$^{-3}$ resided around S atoms while 0.5 $e$ Å$^{-3}$ unmodeled electron density surrounded Zn. S and Zn are renowned for their problematic modeling in charge-density analyses. Indeed, difficulties encountered in modeling the Zn ion are to be expected since transition metals still present a major challenge to the field of charge-density analysis.[31,32] Zn is particularly challenging on account of its $3d^{10}$ electronic configuration which presents valence electron density in a highly spherical form. As such, this renders difficult the effective partitioning of electrons into multipolar terms. Meanwhile, S has a long history of revealing such levels of residual density in charge-density studies,[33–35] and its repeated appearance has been attributed to the diffuse nature of S $d$ orbitals. An exemplification of this issue in another tetrahedral Zn coordination complex is given by Scheins *et al.*[36] where a comparable level of residual electron density was observed around the Zn (0.36 $e$ Å$^{-3}$). S atoms also coordinate to the Zn in that study and show the same 0.2 $e$ Å$^{-3}$ level of residual electron density as our study.

In order to minimize possible artifacts from such residual electron density, special care had been taken over the multipolar refinement of Zn and S (see Supplemental Material[30]). In order to account for their diffuse $d$ orbitals, Zn and S were also modeled up to the hexadecapolar level in the final refinement, while all other nonhydrogen atoms were modeled up to octupolar terms.

The final model was also assessed via the Hirshfeld rigid-bond test,[37] which calculates the difference of mean-square displacement amplitudes (DMSDAs) in the bond directions. The maximum DMSDA for ZTS was 0.0008 Å$^2$ [for S(1)-O(3)] which is sufficiently low that one can be assured of an appropriate deconvolution of all bonding and thermal motion effects.

Least-squares refinement statistics on $F$ for the final multipolar model yielded $R = 0.0179$, $R_w = 0.0167$ ($w = 1/\sigma^2$), a goodness of fit of 1.53, and a data-to-parameter ratio of 29.5.

### C. X-ray constrained wave-function refinement

The x-ray constrained wave-function method devised by Jayatilaka and Grimwood[20] was employed via the program TONTO.[38] Herein, the theoretical molecular wave function of ZTS was first constructed using a standard self-consistent field (SCF) method on a noninteracting molecule using atomic coordinates of ZTS from the multipolar refinement. An associated list of theoretical structure factors were then generated and subjected to a correction for thermal motion. These calculated structure factors were then compared against the experimentally derived x-ray structure factors. A Lagrange multiplier $\lambda$ was employed to minimize the wave-function energy $E$, subject to a penalty function that incorporates the test statistic $\chi^2$. The associated Lagrange equation is

$$L(\mathbf{c},\varepsilon,\lambda) = E(\mathbf{c},\varepsilon) - \lambda[\chi^2(\mathbf{c}) - \Delta], \tag{2}$$

where $\mathbf{c}$ are the molecular-orbital coefficients, $\varepsilon$ are the Lagrange multipliers related to the orthogonality of the orbitals, and $\Delta$ is the desired error in $\chi^2$ which is, in turn, defined as

$$\chi^2 = \frac{1}{N_r - N_p} \sum_{\mathbf{h}}^{N_r} \frac{[F(\mathbf{h}) - F^*(\mathbf{h})]^2}{\sigma^2(\mathbf{h})}, \tag{3}$$

where $N_r$ and $N_p$ are the number of $\mathbf{h}$ reflections and parameters, respectively; $F$ and $F^*$ are the calculated and experimental structure factors, respectively; and $\sigma^2$ is the error in the structure factor.

The $\chi^2$ test statistic was chosen according to its sensitivity to small differences in a fit and its ability to incorporate the experimentally measured error in each structure factor.

Convergence was assured by testing the refinement test statistic, $\chi^2$, against a range of $\lambda$ values. Convergence up to $\lambda = 6$ was possible. However, high gradients from the direct inversion of iterative space (DIIS) method[39] were observed where $\lambda > 4$, implying that those results had converged to excited states. A final choice of $\lambda = 4$ was selected, which had corresponding crystallographic agreement statistics, $R =$ 0.0284, $R_w = 0.0228$, goodness of fit = 2.057, and a test statistic, $\chi^2$, of 4.23.

The optical properties herein were derived from this fitted wave function according to Jayatilaka *et al.*[40,41]

### D. *Ab initio* calculations

*Ab initio* determinations of the optical properties of ZTS were also calculated. These employed Hartree-Fock SCF methods using a 6-31G* basis set, as implemented in the TONTO software.[38] The wave function generated from standard

Hartree-Fock calculations reproduces the experimental x-ray structure factors only slightly better than the IAM model, judging from the respective $\chi^2$ values: 9.44 and 10.41. In contrast, the constrained wave-function method achieves an excellent fit to the data ($\chi^2 = 4.23$), reflecting the inclusion of intermolecular effects that cannot be reproduced by a gas-phase *ab initio* calculation alone.[40]

## III. RESULTS AND DISCUSSION

### A. Topographical analysis of the electron density

#### 1. Topographical features of the electron density

Electron deformation density maps for the primary molecular constituents of ZTS are displayed in Figs. 2–4. These maps represent the difference between a multipolar and spherical atom model, i.e., effectively showing the nature of bonding density and electronic polarization ensuing in a given cross section of the molecule. The spherical nature of Zn, evident in Fig. 2, has already been commented upon. The O- and S-bound ligand coordination, however, is highly directional since lone pair electron densities from O and S donate their charge into empty $4s$ and $4p$ orbitals of the $Zn^{2+}$ ion. Such dative bonding

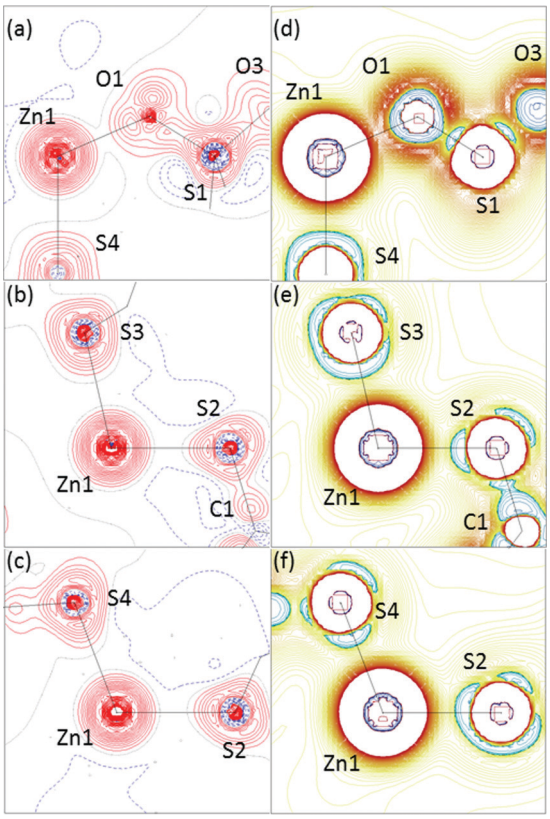


FIG. 2. (Color online) (a)–(c) Electron deformation density and (d)–(f) Laplacian plots that reveal the zinc coordination environment in ZTS. Red lines are positive, blue lines are negative, black lines are zero. A color scale augments the Laplacian maps, since they show local concentrations (blue extreme) and depletions (red extreme) of electronic charge. Contour levels are 0.1 $e$ Å$^{-3}$ linear scaling (densities) and gradient scaling [$0.01(2^n)$, $0 \leqslant n \leqslant 6$]$(2^{n-7}$, $7 \leqslant n \leqslant 13)$[$100(2^{n-14})$, $14 \leqslant n \leqslant 17$] $e$ Å$^{-5}$ (Laplacians).

is most apparent for the O-bound ligand coordination: two of the lone pairs around the O atom are readily resolved [see Fig. 2(a)] and the center of one of them bisects the Zn(1)-O(1) bonding trajectory which joins the two atomic cores (the bond path). Similarly, lone pairs can be seen to bisect the Zn(1)-S bonds [see Figs. 2(b) and 2(c)], although the asphericity of S electron density is more subtle than that of O, owing to the diffuse $d$ orbitals in S. Despite this diffusivity, the triangular features of local maxima which surround the periphery of the $S_{thiourea}$ electron density [bearing in mind the two-dimensional (2D) map projection of Figs. 2(b) and 2(c)] manifest all three lone pairs in these S atoms.

A Laplacian map allows for a better visualization of lone pairs.[42] The Laplacian map displays the second derivative of the electron density at its stationary points, i.e., where $\nabla\rho(r) = 0$, according to the trace of the diagonalized Hessian matrix of spatial curvatures, $\lambda_n$. In the context of a charge-density study, the Laplacian map therefore represents the extent of local concentration or depletion of electronic charge around an atom. Such local concentration is a distinct characteristic of lone pairs and so Laplacian maps are ideal for highlighting them. Figures 2(d)–2(f) present Laplacian maps of the zinc coordination environment. The lone pairs on the $S_{thiourea}$ atoms appear starkly in this presentation with their distinct semicircular profile around a circle of local charge depletion from screened core-shell electrons. Interestingly, the predominance of valence electrons in O renders less contrast in electron-density concentration and depletion. As such, the lone pairs on O(1) are less apparent in a Laplacian map [Fig. 2(d)] compared with its corresponding electron-density map [Fig. 2(a)].

#### 2. Laplacian-based bonding classification

The nature and extent of bonding within ZTS can be quantified by analyzing the Laplacian characteristics at the bond critical point (BCP). A BCP is the point within the bond path where $\nabla\rho(r) = 0$ and the electron density is at a minimum along this bond path but has maximum curvature in the two perpendicular trajectories. This definition renders one positive and two negative eigenvalues $\lambda_n$ as shown by their listing in Table S1 of the Supplemental Material.[30] The normalized difference of these two perpendicular trajectories is defined as the ellipticity of a bond, $\varepsilon$, according to the equation

$$\varepsilon = |\lambda_1 - \lambda_2/\lambda_2| . \tag{4}$$

In effect, $\varepsilon$ describes the level of asphericity in a bond cross section which is perpendicular to the bond path, at the BCP. For example, $\varepsilon = 0$ if the bond comprises purely $\sigma$-bonding, since taking a cross section of a $\sigma$-bond will produce a circle (which, by definition, has zero ellipticity). Meanwhile, double-bonding character will present asphericity in such a bond cross section, owing to the $\pi$-orbital topology; i.e., a nonzero value of $\varepsilon$ will result.

Furthermore, the chemical bonding which dominates a metal coordination environment can be classified via energy densities[43] which are derived from $\rho(r)$ and $\nabla^2\rho(r)$ at each BCP. Therein, the local kinetic energy density at the bond critical point is given by[44]

$$G(r_{BCP}) = \tfrac{3}{10}(3\pi^2)^{2/3}\rho^{5/3}(r_{BCP}) + \tfrac{1}{6}\nabla^2\rho(r_{BCP}), \tag{5}$$

and from the local virial theorem,[45,46] the local potential energy, $V(r_{BCP})$, can be derived:

$$V(r_{BCP}) = \tfrac{1}{4}\nabla^2\rho(r_{BCP}) - 2G(r_{BCP}). \quad (6)$$

The total energy $H(r_{BCP})$ is then given by the sum of the local kinetic and potential energy:

$$H(r_{BCP}) = G(r_{BCP}) + V(r_{BCP}). \quad (7)$$

Evaluations of these three energy densities for each BCP in ZTS are cataloged in Table I. The associated qualifiers for ionic, "polar-shared" (intermediate), and covalent bonding are $\rho(\mathbf{r})$, $\nabla^2(\mathbf{r})$, $G(\mathbf{r})/\rho(\mathbf{r})$, and $H(\mathbf{r})$, according to Table II.[43]

The local source function[47] can also be applied to gauge the level of ionic or covalent bonding character. Once again, this is derived using the Laplacian, this time in concert with a Green's function,[48] according to

$$\rho(\boldsymbol{r}) = \int^{-} (4\pi \cdot |\boldsymbol{r} - \boldsymbol{r}'|^{-1}) \cdot \nabla^2\rho(\boldsymbol{r}') \cdot d\boldsymbol{r}'$$
$$= S(\boldsymbol{r},\Omega) + \sum_{\Omega' \neq \Omega} S(\boldsymbol{r},\Omega')\boldsymbol{r} \in \Omega, \quad (8)$$

where $S(\mathbf{r},\mathbf{\Omega})$ is the source function integrated over the atomic basin of the system, $\mathbf{\Omega}$, surrounding $\mathbf{r}$, with contributions arising from atoms in its own ($\Omega$) and other basins, $\Omega'$. $S(\mathbf{r},\mathbf{\Omega})$ is typically interpreted via the associated parameter, $SF\%$—the contribution of electron density from each atom to a chosen point, $\mathbf{r}$, in a molecule. BCPs are usually selected as $\mathbf{r}$ for a given bond, and $SF\%$ is calculated via $S(\mathbf{r},\mathbf{\Omega})/\rho \times 100$.

Table I presents the $SF\%$ contribution of all Zn, S, and O atoms to the BCPs of all nonhydrogen bonds in ZTS. By mapping electron-density contributions from *all* atoms to *each* bond, $S(\mathbf{r},\mathbf{\Omega})$ is distinct from the above bonding characterizations in taking into account correlated electronic effects. As such, it can be used to identify $\pi$-conjugated (covalent) bonding patterns[49] or electrostatic (ionic) bonding features[50] in molecules, as will be shown below.

Considering the Zn environment in this context, $\nabla^2\rho > 0$, $G(r)/\rho(r) \gg 1$, $H(r)$ is near zero, and $\rho$ values are very small for the Zn-O and all Zn-S bonds, compared to all other bonds, i.e., signaling their dominant ionic nature. $H(r)$ is in fact just positive for Zn-O, while it records a marginally negative value for the Zn-S bonds. This implies that the Zn-O bond is more ionic than the Zn-S bonds, as corroborated by its much larger $|\nabla^2\rho|$ value. This observation is consistent with the expectation of harder (O) and softer (S) Lewis bases. Indeed, the sulfate group is expected to be the predominant negative charge carrier within ZTS. The Laplacian plot (Fig. 3) shows the O lone pair directed towards the zinc according to the expected tetrahedral configuration, lending further evidence that it transfers its electronic charge via the lone pair dative bond. The ellipticity value of Zn-O is effectively zero which indicates that charge transfer is taking place wholly through a $\sigma$-orbital (lone pair) and a spherical (full $d^{10}$) Zn-ion interaction. Indeed, this is corroborated by the fact that the vicinal O(1)-S(1) bond length is somewhat elongated relative to the other sulfate O-S bonds: 1.51 Å versus 1.47 Å (Table I). Indeed, such values represent O-S and O=S bonding, respectively. While the O=S distances are typical for a sulfate group, the O-S bond length lies within

TABLE I. Parameters of all non-hydrogen (3, −1) bond critical points located within the ZTS molecule. $\rho$($e$ Å$^{-3}$) is the electron density; $\nabla^2\rho$ is the Laplacian; $\varepsilon$ is the ellipticity of the bond; $R_{ij}$ is the length (Å) of the bond path between the atoms; $d_1$ and $d_2$ represent the distance (Å) between the first and second atoms specified in the bond column and the critical point, respectively (Ref. 42). $SF\%$ represents the source function contribution of the associated atom to the BCP of the subject bond (Ref. 47).

| Bond | $\rho$ | $\nabla^2\rho$ | $\varepsilon$ | $R_{ij}$ | $d_1$ | $d_2$ | $G(r)$ | $V(r)$ | $H(r)$ | $G(r)/\rho$ | $SF\%$ Zn | $SF\%$ S1 | $SF\%$ S2 | $SF\%$ S3 | $SF\%$ S4 | $SF\%$ O1 | $SF\%$ O2 | $SF\%$ O3 | $SF\%$ O4 |
|---|---|---|---|---|---|---|---|---|---|---|---|---|---|---|---|---|---|---|---|
| Zn(1)-O(1) | 0.529 | 11.992 | 0.01 | 1.9801 | 0.9834 | 0.9967 | 2.992 | −2.987 | 0.00538 | 5.657 | 44.83 | 1.36 | 0.26 | −0.60 | 1.25 | 38.53 | 5.61 | 5.83 | 5.46 |
| S(1)-O(1) | 2.125 | −8.754 | 0.23 | 1.5153 | 0.7008 | 0.8145 | 8.630 | −19.450 | −10.819 | 4.061 | 0.58 | 31.72 | −0.10 | −0.32 | 0.29 | 49.31 | 6.22 | 6.35 | 6.22 |
| S(2)-Zn(1) | 0.313 | 4.866 | 0.19 | 2.3315 | 1.2494 | 1.082 | 1.225 | −1.234 | −0.0090 | 3.915 | 42.62 | 0.76 | 51.97 | 0.55 | −2.35 | −2.40 | 4.26 | 4.51 | 2.67 |
| S(3)-Zn(1) | 0.322 | 5.044 | 0.2 | 2.3322 | 1.254 | 1.0782 | 1.275 | −1.289 | −0.0142 | 3.960 | 42.06 | 0.76 | −0.16 | 47.59 | 0.93 | −2.35 | 2.91 | 4.42 | 3.57 |
| S(4)-Zn(1) | 0.355 | 5.671 | 0.18 | 2.3193 | 1.2541 | 1.0652 | 1.456 | −1.495 | −0.0387 | 4.103 | 41.51 | 0.21 | 0.46 | 0.76 | 39.69 | 1.00 | 3.66 | 5.12 | 2.94 |
| O(2)-S(1) | 2.297 | −3.896 | 0.18 | 1.4691 | 0.7953 | 0.6738 | 10.838 | −22.649 | −11.812 | 4.718 | 0.28 | 35.00 | −0.04 | −0.24 | 0.40 | 4.95 | 48.94 | 5.50 | 5.46 |
| O(3)-S(1) | 2.422 | −12.432 | 0.08 | 1.475 | 0.7765 | 0.6985 | 10.476 | −24.059 | −13.584 | 4.325 | 0.21 | 34.55 | −0.07 | −0.22 | 0.20 | 4.63 | 5.01 | 50.67 | 5.15 |
| O(4)-S(1) | 2.409 | −10.575 | 0.13 | 1.4715 | 0.7859 | 0.6856 | 10.673 | −23.990 | −13.317 | 4.431 | 0.26 | 34.58 | −0.01 | −0.17 | 0.26 | 4.61 | 5.16 | 5.31 | 50.46 |
| N(1)-C(1) | 2.632 | −27.431 | 0.18 | 1.3249 | 0.7287 | 0.5962 | 9.841 | −26.540 | −16.699 | 3.739 | −0.05 | 0.09 | 2.25 | −0.03 | −0.57 | −0.16 | 0.44 | 0.37 | −0.05 |
| N(2)-C(1) | 2.491 | −26.237 | 0.25 | 1.3278 | 0.766 | 0.5619 | 8.777 | −24.112 | −15.336 | 3.523 | −0.03 | 0.08 | 2.85 | −0.01 | −0.58 | −0.17 | 0.34 | 0.28 | −0.02 |
| N(3)-C(2) | 2.53 | −26.737 | 0.22 | 1.3261 | 0.7621 | 0.564 | 9.038 | −24.760 | −15.722 | 3.572 | −0.04 | 0.06 | −0.41 | 2.61 | −0.23 | −0.17 | 0.16 | 0.28 | 0.19 |
| N(4)-C(2) | 2.623 | −27.675 | 0.26 | 1.3257 | 0.7647 | 0.561 | 9.718 | −26.355 | −16.637 | 3.705 | 0.01 | 0.06 | −0.33 | 2.85 | −0.09 | −0.19 | 0.13 | 0.24 | 0.17 |
| N(5)-C(3) | 2.729 | −24.76 | 0.12 | 1.3303 | 0.7444 | 0.586 | 11.182 | −28.555 | −17.372 | 4.098 | 0.12 | 0.09 | −0.05 | −0.11 | 3.41 | 0.10 | 0.03 | 0.46 | 0.29 |
| N(6)-C(3) | 2.573 | −25.88 | 0.24 | 1.3246 | 0.8002 | 0.5244 | 9.565 | −25.600 | −16.035 | 3.717 | 0.11 | 0.09 | −0.04 | −0.06 | 4.00 | 0.15 | 0.02 | 0.44 | 0.21 |
| C(1)-S(2) | 1.286 | −1.642 | 0.24 | 1.7286 | 0.8693 | 0.8593 | 4.095 | −8.600 | −4.505 | 3.184 | 0.01 | 0.16 | 54.32 | −0.06 | −1.20 | −0.67 | 0.80 | 0.71 | 0.15 |
| C(2)-S(3) | 1.323 | −1.743 | 0.24 | 1.7408 | 0.8718 | 0.869 | 4.290 | −9.015 | −4.725 | 3.242 | 0.28 | 0.13 | −0.62 | 52.73 | −0.08 | −0.54 | 0.33 | 0.64 | 0.49 |
| C(3)-S(4) | 1.45 | −1.09 | 0.28 | 1.7335 | 0.8615 | 0.872 | 5.154 | −10.581 | −5.427 | 3.555 | 0.46 | 0.12 | −0.09 | −0.08 | 51.64 | 0.26 | 0.34 | 0.96 | 0.45 |

TABLE II. A summary of the bond-type classifications according to energy density descriptors.

| Bond type | $\rho(\mathbf{r})$ | $\nabla^2(\mathbf{r})$ | $G(\mathbf{r})/\rho(\mathbf{r})$ | $H(\mathbf{r})$ |
|---|---|---|---|---|
| Ionic | Small | $>0$ | $\geqslant 1$ | $>0$ |
| Polar shared | Large | Arbitrary | $\geqslant 1$ | $<0$ |
| Covalent | Large | $<0$ | $<1$ | $<0$ |

the upper quartile of all known sulfate bonds that are bound to a metal [cf. $\bar{x} \pm \sigma = 1.487 \pm 0.026$ Å from a sample, $N = 166$, with range 1.267–1.554 Å; upper quartile: 1.500 Å (Ref. 51)]. This means that O-S has lost a significant level of electron density to the Zn-S interaction, yet, this loss must originate from $\sigma$-orbital electrons, since its $\pi$-electron density is the greatest out of all S-O bonds, as judged by $\varepsilon$. Therefore, the O in this bond is negatively charged.

The rest of the sulfate group is essentially neutral as governed by the S=O bonding, although there are hints of resonance effects, e.g., the shortest S=O bond (and commensurately highest $\varepsilon$ value) simultaneously exhibiting modest covalent character, as judged by the much less negative $\nabla^2\rho$ value of O(2) = S(1) relative to that of other O=S bonds. This would stand to reason if a charged S=O resonance form persists. The longest S=O bond, S(1) = O(3), also has the smallest $\varepsilon$ value out of the three such bonds. This can all be accounted for by its involvement in the very short aforementioned hydrogen bond. All O-S BCPs lie closer to the S than O; this means that electron density is polarized towards the oxygen atoms, as anticipated.

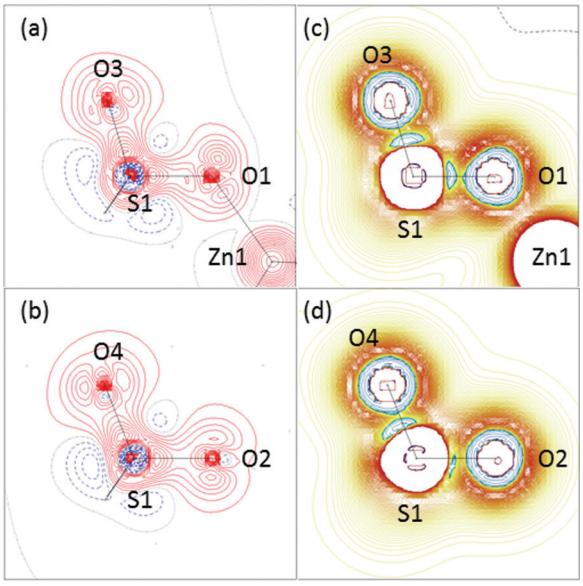


FIG. 3. (Color online) (a), (b) Electron deformation density and (c), (d) Laplacian plots that reveal the sulfate bonding within ZTS. Red lines are positive, blue lines are negative, black lines are zero. A color scale augments the Laplacian maps, since they show local concentrations (blue extreme) and depletions (red extreme) of electronic charge. Contour levels are 0.1 $e$ Å$^{-3}$ linear scaling (densities) and gradient scaling [$0.01(2^n)$,$0 \leqslant n \leqslant 6$]($2^{n-7}$, $7 \leqslant n \leqslant 13$)[$100(2^{n-14})$, $14 \leqslant n \leqslant 17$] e Å$^{-5}$ (Laplacians).

The bonding nature of the $SO_4^{2-}$ ion in the compound, $K_2SO_4$, has recently been questioned via another charge-density study,[52] so a comparison to ZTS was sought. There is no analogous S(1)-O(1) single-bond length in $K_2SO_4$, presumably since this is bound to the strongly ionic Zn(1)-O(1) in ZTS owing to the full $d^{10}$ electron configuration of Zn. The other S=O bond lengths in ZTS are, however, very similar to those in the experimentally determined $K_2SO_4$. $\nabla^2\rho$ values for S=O bonds do differ between experiments: Those in ZTS are an order of magnitude larger than those for $K_2SO_4$. That said, $\nabla^2\rho$ values derived from their density functional theory are a fair match to S=O bonds in ZTS. Given this discrepancy and known concerns of the employment of $\nabla^2\rho$ alone as a bonding descriptor, local source functions from each study were compared. The O2, O3, and O4 $SF\%$ contributions to each of the three S=O bonds in ZTS (Table I) are practically identical to those in $K_2SO_4$ (50%; see Table 5 of Ref. 51). However, the corresponding S $SF\%$ contributions are consistently larger for ZTS (35%), versus 29% in $K_2SO_4$. The greater difference between O and S $SF\%$ in ZTS is indicative of its more polarized S=O bonding. Considering correlated electronic effects in ZTS, all oxygen atoms contribute an $SF\%$ of 5% to adjoining O-S bonds; this contribution extends from the S=O bond through to the S(1)-O(1) and Zn(1)-O(1) bonds. However, only O2, O3, and O4 provide a significant $SF\%$ of 3%–5% to Zn-S bonds, a feature that is distinctly absent in O1. Such an absence is consistent with nodal effects associated with an ionic, negatively charged O-S bond. Meanwhile, the more extended charge delocalization from S=O bonds is consistent with charge transfer and resonant S=O bonding, on the one hand, and dominant ionic Zn-S characteristics, on the other hand.

The less ionic Zn-S bonds, relative to Zn-O, could also be quantified further using the local source function. Indeed, the marginally negative $H(r)$ value, mentioned earlier, is concurrent with otherwise dominant ionic energy density classifiers. This suggests an ambiguity that could reflect a mixed bonding character.

Considering the basic features of their BCPs first, Zn-S bonds are all located closer to Zn than S, by the same extent ($d_1/d_2$ ratios between Zn-S bonds are essentially identical). Their elliptical values are identical within error, and are representative of a significant level of aspherical orbital bonding contribution; the diffuse S electrons are presumably the most likely origin of this asphericity since the zinc Laplacian topography appears quite spherical (Fig. 2).

Considering their $SF\%$ characteristics (Table I), Zn1 contributes a consistent $SF\%$ of 42%–43% to all Zn-S BCPs. S2 and S3 provide more electron density (52%, 48%) to the bond than Zn, providing a significant level of polarization. In contrast, Zn(1)-S(4) bears almost no polarization since Zn and S4 $SF\%$ values are almost identical ($SF\%$ for S4 is 40%). Regarding nondirectly bonded $SF\%$ contributions, a modest amount emanates from O2, O3, and O4, as mentioned above. $SF\%$ values for the N and C thiourea groups are also significant; these values are given in the Supplemental Material[30] but their salient contributions are summarized here. Any given nitrogen of the thiourea groups provides up to 6% of the Zn-S bonding density. The largest N $SF\%$ contribution to S2 or S3 arises from a N that resides in the thiourea group

associated with the corresponding S; this is as one might expect from a $\pi$-conjugated thiourea ligand. However, $SF\%$ values from nitrogen atoms belonging to *different* thiourea groups, are comparable for Zn(1)-S(2) and Zn(1)-S(3), culminating in a total 13% and 17% $SF\%$ contribution, respectively. In contrast, all C $SF\%$ values relating to these two Zn-S bonds are null or negative. This indiscriminant spread of N electron density donating to S2 and S3 with nodal carbons is consistent with ionic bonding; the direct-bond polarization in Zn(1)-S(2) and Zn(1)-S(3) corroborates this bonding assignment. In contrast, the nonpolarized Zn(1)-S(4) bond receives nitrogen $SF\%$ contributions very exclusively from N5 and N6, i.e., only those nitrogen atoms that are directly bonded to C3 which, in turn, bonds to S4, as per $\pi$-conjugation expectations of a thiourea ligand. C3 also affords a non-negligible (2%), carbon exclusive $SF\%$, to Zn(1)-S(4). All of these indicators point to a selectively covalent tendency of the Zn(1)-S(4) bond. It is also interesting to observe that atomic charges of ZTS, similarly derived from this charge-density study (see Supplemental Material[30]), reveal consistent manifestations of ionic Zn(1)-S(2) and Zn(1)-S(3), but covalent Zn(1)-S(4).

These differences in Zn-S bonding character are very localized, as evidenced by the $SF\%$ contributions for all thiourea BCPs; those from each ligand are essentially identical. Indeed, all thiourea groups also display very similar charge-density distributions. This similarity is categorized visually via their electron deformation densities (Fig. 4). The constituent $\nabla^2\rho$ values for a given bond type are also very similar; cf. $\overline{\nabla^2\rho} \pm \sigma = -1.492 \pm 0.352\ e\,\text{Å}^{-5}$ (S-C); $-26.453 \pm 1.074\,e\,\text{Å}^{-5}$ (C-N); $-29.460 \pm 5.494$ (N-H). Even ellipticity values, which are generally much more sensitive to small perturbations, are similar with one exception: $\varepsilon = 0.12$ for C(3)-N(5); cf. $\bar{\varepsilon} + \sigma = 0.21 \pm 0.05$ for all C-N bonds in the other two thiourea ligands. This exception is, however, consistent with the fact that C(3)-N(5) is longer, and therefore weaker, than the other C-N bonds; therefore a lower $\varepsilon$ value results from less $\pi$-electron-density overlap.

We anticipate that the origin of this significantly long bond owes itself to hydrogen-bonding effects: the C(3)-N(5) bond is associated with the strongest (by some margin) hydrogen bond in ZTS, N(5)-H(5B)$\cdots$O(3) [1.815(1) Å (Ref. 15)]. This value is short in itself; indeed, only five shorter N-H$_{(\text{thiourea})}\cdots$O hydrogen bonds have ever been reported[53–57] out of all 668 published crystal structures that contain this nonbonded contact [below the sum of O and H van der Waals radii threshold,[58,59] as sourced from the Cambridge Structural Database using CONQUEST 1.14 (Ref. 51) and VISTA (Ref. 60)]. This N-H$_{(\text{thiourea})}\cdots$O hydrogen-bond is part of an extensive network of nonbonded contacts in ZTS (Ref. 15) that serves to stabilize the molecule.

No electronic polarization is evident in the S-C bonds, as judged by their centrally positioned BCPs. Although covalent bonding dominates [$\nabla^2\rho < 0$, $H(r) < 0$], these bonds can be considered as "polar shared," i.e., they are fairly well stabilized by covalent *and* ionic contributions, since $\nabla^2\rho$ is only slightly negative, $G(r)/\rho(r) > 0$, and $\rho$ is moderate. That said, one should be careful how far one extends the application of these energy density parameters, since the derivation of $G(r)$ via the local virial theorem only holds well for closed-shell interactions.[44] All energy densities are given for completeness in Table I. However, for internal covalent bonds, it is generally considered more appropriate to simply

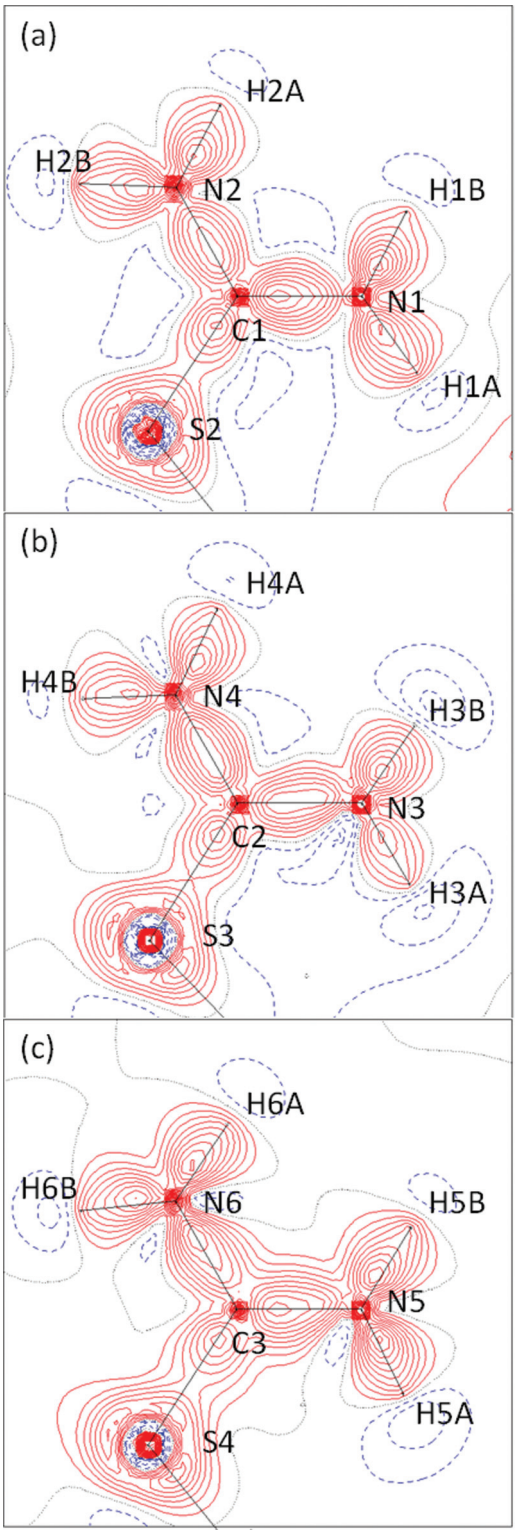


FIG. 4. (Color online) Electron deformation density plots of the thiourea constituents of ZTS. These represent the difference between a multipolar and spherical atom model, i.e., effectively showing the level of bonding electron density and electronic polarization in this part of the molecule. Red lines are positive (actual electron density), blue lines are negative, black lines are zero; contour levels are $0.1\ e\,\text{Å}^{-3}$.

use the sign and magnitude of the Laplacian for each BCP to indicate, respectively, the nature and extent of chemical bonding.[61] Other topological descriptors are also helpful here. For example, there is significant $\pi$-electron density between the bond ($\bar{\varepsilon} = 0.25 \pm 0.02$) such that it can be considered to be a S=C double-bond.

The exclusive use of the Laplacian for bond classification is even more relevant for C-N and N-H bonds; these are effectively covalent (large negative $\nabla^2\rho$ values) and are polarized. The C-N bonding electrons are polarized towards the nitrogen atom (BCP closer to the carbon atom), in accordance with basic electronegativity expectations. The same trend is seen in the N-H bonds although here the level of polarization toward the N atom is more pronounced.

### B. Relationship to optical properties

#### *1. Categorizing the NLO origins by charge transfer*

Consideration of these topological electronic characteristics provides a very helpful insight into the structural mechanism by which the nonlinear optical phenomenon is conveyed. The nature of this mechanism is not immediately clear in a metalorganic compound since NLO activity in inorganic and organic materials emanates from different structural origins. For example, the electronic hyperpolarizability required for second-harmonic generation is caused by ionic displacement in an inorganic material; in contrast, SHG from an organic material emanates from electronic charge transfer across a key part of the molecule. One might therefore intuit that the structural origins of NLO behavior in a metalorganic compound, such as ZTS, would manifest as a hybrid of these inorganic and organic aspects.

The valence bonding characteristics revealed by this charge-density study enable an assessment of this intuition. While this study probes the molecule in the ground state such that one cannot actually observe ionic displacement or charge transfer as it happens, one can readily infer its propensity for NLO behavior and its nature thereof. For example, ionic displacement will only occur if a part of the molecule is suitably ionic while molecular charge transfer requires electronic delocalization pathways through covalent $\pi$-bonding. So the effective question becomes as follows: to what extent is ZTS ionic or covalent, and how are these bonding types distributed, i.e., what parts of the molecule are responsible for which type of NLO structural origin.

Summarizing the relevant findings of the Laplacian-based valence-bonding classification from Sec. III A 2, the energy densities associated with the zinc ion showed that this is the primary center of ionic bonding. The diffuse nature of S *d* electrons offers larruping good opportunities for orbital overlap; meanwhile, the $\varepsilon$ and $SF\%$ values for these bonds evidence $\pi$-electron density therein. As such, there is a clear pathway for electronic charge transfer from S to Zn; indeed, the BCPs for Zn-S reveal a distinct polarization towards the zinc. The refined charge on zinc also shows that its formal charge is partly stabilized by a reductive charge transfer. This stabilization arises from the overall single negative charge emanating from the sulfate group; not two as one might intuit from basic chemical considerations of isolated $SO_4^{2-}$ ions. The electron-density distribution of the thiourea groups remains unaffected by their proximity to zinc. Indeed, BCPs lie very centrally within the S = C bonds, covalent and ionic characteristics are well balanced ("polar-shared" bonding), and there is no net charge. Indeed, the high similarity between electron-density distributions of all three thiourea groups is characteristic of such isolated behavior, as it would otherwise be affected by the electronic asymmetry of the molecule. Moreover, electronic polarization within these groups is very typical of an isolated thiourea group: their distributions are qualitatively similar to those of charge-density studies on urea and thiourea.[62,63] The other constituent part of the molecule, the coordinated sulfate ion, binds to Zn in an ionic fashion, and otherwise exhibits largely resonant bonding.

The thiourea groups must therefore represent the primary $\pi$-conjugated covalent contribution to the NLO behavior (i.e., of an organic nature), and do so as three discrete units. Interestingly, these units are configurationally bound by pseudo-$C_3$ (threefold rotational) molecular point-group symmetry. Such threefold symmetry in a tetrahedral manifold, where an electron donor (in this case, Zn) lies at the central point, is commensurate with octupolar NLO phenomena.[1] Such octupolar topologies suggest that the hyperpolarizability tensorial coefficients, $\boldsymbol{\beta_{ijk}}$, for ZTS will be somewhat three dimensional (3D) in nature,[1–3] as we confirm in Sec. III B 2. This contrasts with the more typical situation in planar organic molecules where >90% of the total hyperpolarizability appears to originate from $\boldsymbol{\beta_{zzz}}$ coefficient.[21]

Overall, this analysis can be used to reconcile the hypothesis that the NLO origins of a metalorganic compound, such as ZTS, are a hybrid of organic and inorganic manifestations. Clearly, there is only a single NLO effect observed and so our partitioning of ZTS into ionic (inorganic) and covalent (organic) contributions must be drawn together and seen as an overall model of "charge-transfer molecular graph." Figure 5 presents this model as a tripod of charge transfer passing from the thiourea groups to the metal, on the one hand—and a sulfate group having an ionic interaction with the metal, while stabilizing a negative charge, on the other. The discrete

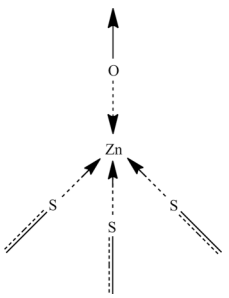


FIG. 5. The overall model of "charge-transfer molecular graph" descriptor. This provides a snapshot illustration of the nature of charge transfer ensuing in the molecule in terms of the respective ionic and covalent contributions. The arrows show the direction to which the electronic charge is polarized in this tetrahedral molecule. Solid lines represent covalent bonding and dashed lines represent ionic bonding, while bonds displaying both covalent and ionic character are marked with both solid and dashed lines. No arrowhead on a line indicates no net charge transfer in the bond immediate to the labeled atom.

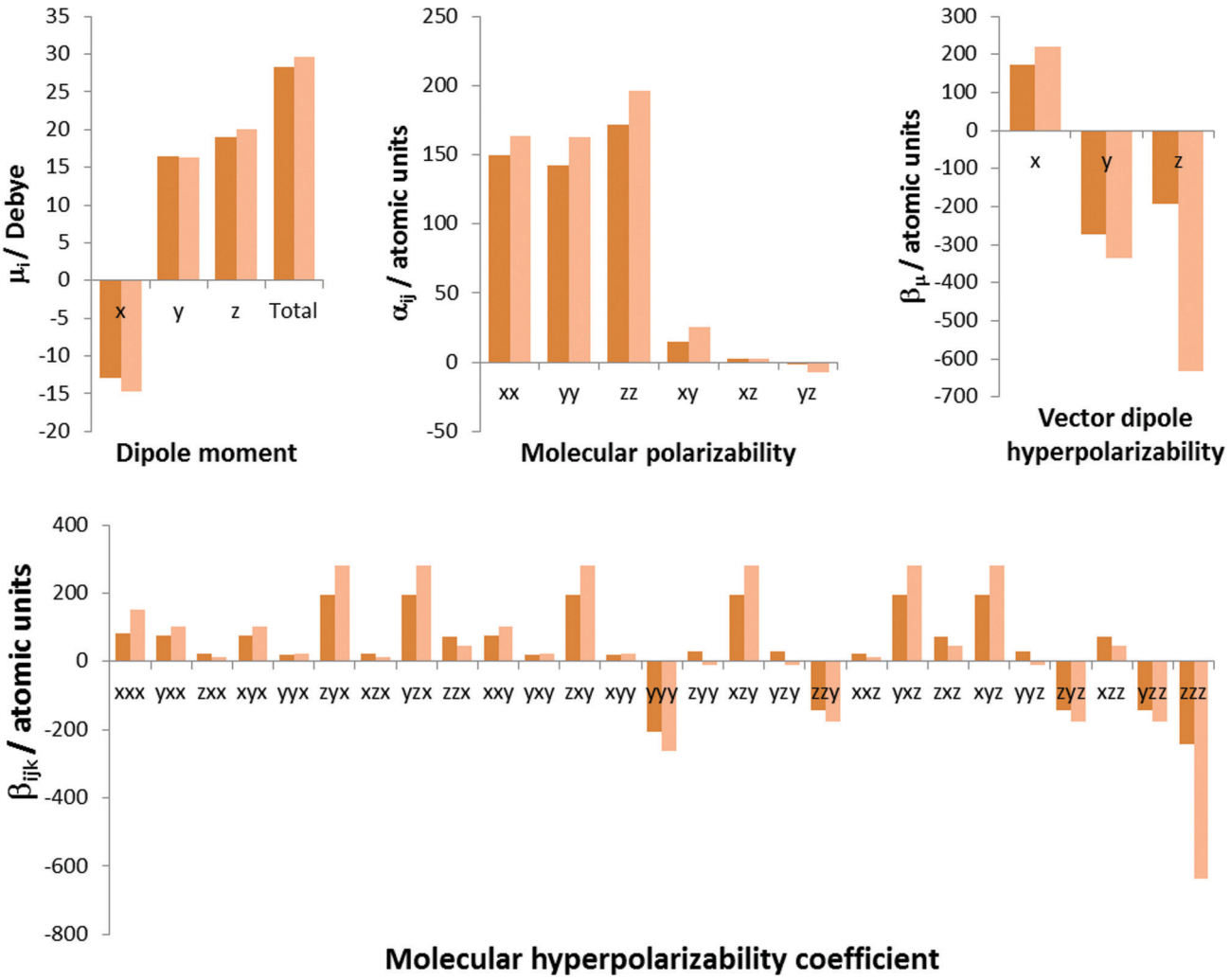


FIG. 6. (Color online) Molecular dipole moment ($\boldsymbol{\mu}_i$), linear polarizability ($\boldsymbol{\alpha}_{ij}$), first hyperpolarizability ($\boldsymbol{\beta}_{ijk}$), and vector dipole hyperpolarizability ($\boldsymbol{\beta}_{\mu}$) coefficients for ZTS, as derived from gas-phase *ab initio* calculations (dark color) and wave-function fitting of the x-ray diffraction data (light color).

covalent and ionic components lie contiguous such that overall continuity of molecular charge transfer is ensured.

### 2. *Evaluating $\mu_i$, $\alpha_{ij}$, $\beta_{ijk}$ coefficients from molecular charge densities*

As mentioned earlier (Sec. I and Ref. 19), the nonhomogeneous nature of electronic distribution in ZTS places concern on the reliability of solid-state calculations of $\boldsymbol{\mu}_i$, $\boldsymbol{\alpha}_{ij}$, and $\boldsymbol{\beta}_{ijk}$ for ZTS, when taken from multipolar moments that are derived from a charge-density study. Moreover, there is additional concern given that the already sensitive optical property calculations will be affected markedly by the significant residual electron density surrounding the zinc ion. Nevertheless, a speculative calculation was undertaken using the Stockholder method of atomic partitioning.[64] In tandem, complementary *ab initio* calculations and x-ray constrained wave-function refinement derivations of these optical properties were also performed.

As expected, evaluations of $\boldsymbol{\mu}_i$, $\boldsymbol{\alpha}_{ij}$, and $\boldsymbol{\beta}_{ijk}$ from the charge-density study do not appear to be sensible when compared with the *ab initio* and constrained wave-function refinement evaluations. Indeed, the latter two evaluations agree with each other well, both the magnitude and direction (see Fig. 6). In stark contrast, the charge-density-derived values differ from them by up to two orders of magnitude and exhibit completely different trends in the direction of the various tensors.

That said, the correct result should not simply be chosen on the basis that the consistency of two methods is better than one. This is especially true where *ab initio* calculations were conducted in the gas phase while the multipolar fitting produces solid-state values; the constrained wave-function method is effectively a hybrid in this sense. Fortunately, the constrained wave-function results in this study could be verified via the experimental report of the refractive index, $n$, of ZTS.[61] Constrained wave-function refinement has been shown to be effective in calculating the value of $n$ from the linear polarizability.[40] While the focus of this paper is on the nonlinear optical aspects of ZTS, $\boldsymbol{\beta}_{ijk}$ is a higher-order coefficient in the power series than $\boldsymbol{\alpha}_{ij}$ [see Eq. (1)]; therefore experimental results which validate $\boldsymbol{\alpha}_{ij}$ also give

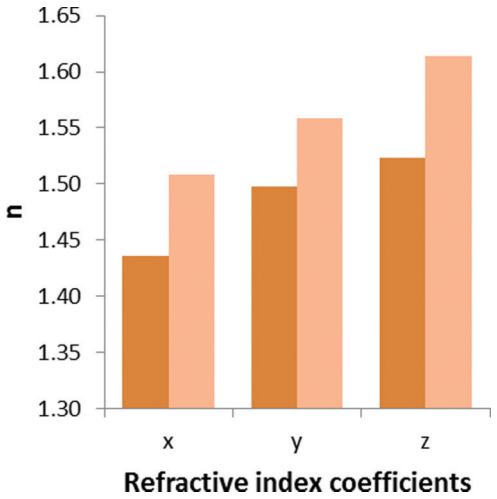


FIG. 7. (Color online) The refractive index coefficient, $\mathbf{n_i}$, for ZTS, as derived from gas-phase *ab initio* calculations (dark color) and wave-function fitting of the x-ray diffraction data (light color).

good confidence to the same implicit calculations used to evaluate $\boldsymbol{\beta_{ijk}}$. Using the RLFTn approximation within TONTO, the refractive index coefficients, $\mathbf{n_i}$, were evaluated from the linear polarizability, $\boldsymbol{\alpha_{ij}}$, at zero frequency (static values); see Fig. 7. The linear refractive index of ZTS was available at two wavelengths: 1.391 at 1100 nm and 1.453 at 632.8 nm.[65] Optical dispersion was accounted for by performing a linear extrapolation of these experimental data to zero frequency, affording a static refractive index, $n = 1.537$. This value is in remarkable agreement with the refractive indices derived from the linear polarizability obtained by constrained wave-function refinement; see Fig. 7. It is noteworthy that the refractive indices derived herein are all comparable albeit following a consistent trend, $n_z > n_y > n_x$, i.e., displaying biaxial optical activity that is also observed by experiment.[65] These comparable values stand to reason given that the principal $xx$, $yy$, $zz$ terms of the linear polarizability are all similarly significant, with $zz$ being slightly larger. Meanwhile, the cross terms of $\boldsymbol{\alpha_{ij}}$ are notable by their negligible contributions. The agreement to experiment is actually significantly better for the constrained wave-function refinement results compared with those from the *ab initio* study. This is presumably a consequence of the fact that the constrained wave-function method takes into account solid-state effects, given the dependence of experimental structure factors from crystallographic data, i.e., from a solid-state sample, as per the same phase of the sample for refractive index measurements. Indeed, recent work[40] has demonstrated that the solid-state crystal-field effects are incorporated well into the constrained wave-function result, even to the extent that weak forces such as intermolecular interactions can be evaluated reliably. This contrasts with the gas-phase *ab initio* calculations. Overall, the normalization of these calculations to experimental optical measurements strongly corroborates the initial thesis that the *ab initio* and constrained wave-function methods offer the two reliable sets of results.

This finding advocates the use of the charge-density data to derive optical properties in nonhomogeneous compounds, such as metalorganics, but *only* within the confines of the constrained wave-function method. Such a constraint then yields good confidence in the coefficient evaluations, pending *ab initio* calculations are broadly similar, as in this case.

It should be noted that the refractive index has been used for normalizing these results to experiment rather than the hyperpolarizability coefficient itself, even though that is the primary interest of this paper. On the one hand, an experimental value of $\boldsymbol{\beta_{ijk}}$ was not available and, even if it was, it would not be available in the solid state. Experimental options to evaluate $\boldsymbol{\beta_{ijk}}$ are conducted on the material when in the solution phase, by hyper-Rayleigh scattering (HRS),[66] or they can be embedded within an electrically poled thin-film polymer environment and, in that case, $\boldsymbol{\beta_{ijk}}$ is measured indirectly via related optical parameters [using electric-field-induced second-harmonic (EFISH) generation].[67] Meanwhile, the reflective index is measured in the solid state. On the other hand, all experimental measurements of $\boldsymbol{\beta_{ijk}}$ are susceptible to very significant levels of error: a standard deviation that is 10%–30% of the actual $\boldsymbol{\beta_{ijk}}$ value is common.[68] In stark contrast, the refractive index is usually affordable to an accuracy of its third decimal place. Considering these factors, $n$ is clearly the superior choice for experimentally validating the results herein.

Overall, the *ab initio* and x-ray constrained wave-function results show that all optical coefficients are largest in the **Z** direction. This is consistent with the majority of organic NLO molecules; indeed, >90% of the total hyperpolarizability is generally considered to emanate from $\boldsymbol{\beta_{zzz}}$ in dipolar molecules;[21] there, though, the charge-transfer pathways in the organic molecules are typically two dimensional. Yet, as discussed in Sec. III B 1, ZTS exhibits charge transfer in a distinctly three-dimensional fashion. Nevertheless, $\boldsymbol{\beta_{zzz}}$ still presents by far the largest contribution to the overall $\boldsymbol{\beta}$ value. The principal orthogonal term, $\boldsymbol{\beta_{yyy}}$, is the second largest coefficient. The only other significant $\boldsymbol{\beta}$ values that propagate in the same sense are the associated cross terms, $\boldsymbol{\beta_{yzz}}$, $\boldsymbol{\beta_{zyz}}$, and $\boldsymbol{\beta_{zzy}}$. These terms are identical to each other owing to the imposition of Kleinman symmetry.[69] This equates all $\boldsymbol{\beta_{ijk}}$ coefficients that are (ijk) permutations of each other, i.e., (yzz) in this case. While there is a growing number of materials whose nonlinear optical behavior has been shown to deviate from Kleinman symmetry,[70] even far from resonance conditions, the zero-frequency nature of the $\boldsymbol{\beta}$ values derived herein preclude optical dispersion effects from violating this symmetry condition.

The only comparable $\boldsymbol{\beta}$ contributions that propagate in the opposite sense to the aforementioned $\boldsymbol{\beta}$ tensors are the six that are also related by cyclic permutation, (xyz), another manifestation of Kleinman symmetry. Thereafter, the $\boldsymbol{\beta_{xxx}}$ value lies just ahead of the remaining, relatively minor, contributions.

The overall tensorial contribution to $\boldsymbol{\beta}$ in ZTS is therefore markedly three dimensional in nature. First of all, this attests to the 3D charge-transfer characteristics of the molecule (as detailed in Sec. III B 1), which are fundamentally related to the NLO origins of ZTS. Secondly, the 3D nature of $\boldsymbol{\beta}$ in ZTS, taken together with the pseudo-$C_3$ point-group symmetry of the ZTS molecule, suggests that octupolar ($\boldsymbol{\beta_{J=3}}$) as well as dipolar ($\boldsymbol{\beta_{J=1}}$) hyperpolarizability contributions will be

noteworthy (where J is the $m = +1, 0, -1$ subspace of spherical harmonics); indeed, the augmenting terms for $\boldsymbol{\beta}_{\mathbf{J=3}}$ in perfect $C_3$ symmetry ($\boldsymbol{\beta}_{xxx}$, $\boldsymbol{\beta}_{yyy}$, and $\boldsymbol{\beta}_{zzz}$) are all significant for ZTS.[1]

Since it is common to electrically pole NLO materials, it is helpful to also consider the hyperpolarizability vector that lies along that of the molecular dipole, i.e., the vector dipole hyperpolarizability, $\boldsymbol{\beta}_{\mu}$. Compared with the respective hyperpolarizability coefficients, $\boldsymbol{\beta}_{\mu}$ is similarly dominant in the $z$ direction, most notably in the x-ray constrained wave-function refinement results. Although the secondary $\boldsymbol{\beta}_{\mu}$ contribution lies in the $y$ direction, the vector dipole hyperpolarizability is somewhat significant in both $y$ and $z$ directions, albeit distinguished by sign. This illustrates a distinctly three-dimensional nature of the NLO phenomenon in ZTS. These trends in vector dipole hyperpolarizability follow essentially the same as that of the molecular dipole moment, which stands to reason since it is upon this which $\boldsymbol{\beta}$ is herein aligned; effects on the resulting $\boldsymbol{\beta}_{\mu}$ are therefore essentially summative.

Furthermore, the overall value of the molecular dipole moment is substantial: 28.3 and 29.7 D from the *ab initio* and constrained wave-function results, respectively. Such values compare well with solid-state derivations of $\boldsymbol{\mu}_{\mathbf{total}}$ in highly polarizable organic nonlinear optical molecules.[71–74] This supports the idea that the NLO origins in ZTS arise largely from charge-transfer (i.e., organic) characteristics. It is interesting to note that $\boldsymbol{\mu}_{\mathbf{total}}$ of ZTS is enhanced, but only by a small amount, when moving from gas-phase *ab initio* results to those of constrained wave-function refinement. Given that solid-state crystal-field effects are incorporated well into the constrained wave-function result,[40] one therefore presumes that the gas-to-solid phase enhancement in $\boldsymbol{\mu}_{\mathbf{total}}$ for ZTS is naturally small.

In general terms, a consistent trend is observed wherein the optical properties derived from the x-ray constrained wave-function method are greater than those from *ab initio* calculations. While the differences between them are small in the lower-order moments, such as the dipole and second moments, they become more and more apparent as the order of the moment increases. The linear polarizability coefficients and their associated refractive indices show significant differences, while the first hyperpolarizability and associated vector dipole hyperpolarizability show marked differences, especially for coefficients projected along the $z$ direction. This consistent enhancement of optical property values from the refined constrained wave-function model, relative to *ab initio* calculations, lends further evidence to its successful incorporation of solid-state crystal-field effects. The especially marked enhancement of hyperpolarizability along the $z$ direction in the constrained wave-function results could have several origins: perhaps some sort of manifestation of systematic error carried through from the x-ray-derived structure factors; indeed, the worst disparities between the charge-density-derived (hyper)polarizabilities and those from the chosen methods were in the $z$ direction. Alternatively, supramolecular effects could be responsible. Indeed, crystal-field effects appear to affect the overall enhancement in optical properties of organic NLO materials;[71,75] ZTS displays an extensive network of hydrogen bonding[15] and, as we have shown herein, presents strongly organic charge-transfer characteristics.

## IV. CONCLUSIONS

A topological analysis of the molecular charge density in ZTS has provided a very detailed description of the chemical bonding, across its constituent molecular parts. In turn, this has enabled one to categorize the nature of charge transfer in ZTS. This has shown that the NLO origins of ZTS are distinctly organic, with the effects of polarization from ionic contributions being very contained—its influence does not extend beyond the coordinative atom bound to the metal ion.

The molecular dipole and (hyper)polarizability coefficients of ZTS were calculated in order to judge its intrinsic NLO potential at the quantum level. Here, the charge-density study did not perform well on its own account, which was not so surprising given the nonhomogeneous nature of the molecule. The results do, however, show that when theoretical structure factors are refined against those of the charge-density data, this constraint proves very powerful. Such findings strongly advocate the use of so-called x-ray constrained wave-function refinement to determine optical properties from a molecular perspective; supporting gas-phase *ab initio* calculations are shown to be helpful for verification purposes. This study used the ability of the constrained wave-function method to calculate the refractive index, $n$, as a means by which one could validate the calculations of $\boldsymbol{\mu}_{\mathbf{i}}$, $\boldsymbol{\alpha}_{\mathbf{ij}}$, and $\boldsymbol{\beta}_{\mathbf{ijk}}$ to experiment. An experimental measure of the refractive index compared remarkably well with that derived from constrained wave-function refinement, where $\mathbf{n}_{\mathbf{i}}$ was derived from $\boldsymbol{\alpha}_{\mathbf{ij}}$. While NLO properties were the focus of this study, this result also propounds the use of wave-function fitting to calculate $n$ where the refractive index is of primary interest in a study. Indeed, other studies that target such calculations directly is the subject of related work.[41]

The results have revealed that ZTS possesses a substantial molecular dipole moment of 28.3 and 29.7 D in the gas and solid state, respectively. The vector dipole hyperpolarizability, $\boldsymbol{\beta}_{\mu}$, is therefore augmented substantially relative to $\boldsymbol{\beta}_{\mathbf{ijk}}$. This suggests that ZTS would perform well in thin-film technologies where ZTS is subject to electrical poling. While the application of ZTS has focused on single-crystal forms, extending the application of ZTS to its incorporation within a polymer poling process might prove useful. Indeed, polymer poling is, in any case, a very commonly used process in the field of nonlinear optics.

That said, one should not ignore the three-dimensional nature of $\boldsymbol{\beta}_{\mathbf{ijk}}$ in ZTS which is also highlighted by this work, and which indicates marked octupolar as well as dipolar NLO activity. Given these findings, it would be very helpful to investigate further the nature of this octupolar contribution, via experiments. HRS stands to be very useful in this regard, as it can generate an experimental measure of all 27 tensorial coefficients in a material. While HRS is a solution-based technique, the close match between gas-phase *ab initio* and wave-function fitting (effectively solid state) results herein demonstrate that $\boldsymbol{\beta}_{\mathbf{ijk}}$ will not alter substantially owing to a change in phase.

Looking ahead, given the increasing drive in nanotechnology, one could even explore the optimization of the 3D NLO characteristics of ZTS through the judicious design of novel 3D functional material architectures. The fact that ZTS is a metalorganic compound means that it could also be chemically incorporated into much larger nanostructure frameworks, the classic case being metalorganic frameworks (MOFs). In this sense, it is of course a particular asset that ZTS has already proven itself as a rare case of a chemically stable and industrially promising metalorganic NLO material.

Overall, these results on ZTS will hopefully help towards affording a better understanding of structure-property relationships in metalorganic NLO materials. Thence, the molecular building blocks can be put in place to systematically design new functional NLO materials. This leads to the ultimate goal of being able to "molecularly engineer" designer NLO materials to suit a given device application.


## ACKNOWLEDGMENTS

The authors wish to thank Professor Dylan Jayatilaka and Professor Mark Spackman of the University of Western Australia, Crawley, Perth, for the use of the RLFTn approach that they have implemented in TONTO. All authors are also grateful to Professor John Sherwood and Evelyn Shepherd, University of Strathclyde, UK, for supplying the ZTS crystals, to Professor Judith Howard for access to x-ray diffraction facilities at the University of Durham, UK, and to Dima Yufit (Durham) and Shamus Husheer (Cambridge) for assistance with x-ray data collection and reduction. J.M.C. wishes to thank the Royal Society for its support through a University Research Fellowship, and NSERC for Discovery Grant No. 355708. D.D.H. is indebted to The Winston Churchill Foundation of the United States for providing support through an eponymous scholarship.


*Corresponding author: jmc61@cam.ac.uk


[1] N. J. Long, Angew. Chem., Int. Ed. Engl. **34**, 21 (1995).
[2] J. M. Cole, Philos. Trans. R. Soc., A **361**, 2751 (2003).
[3] J. Zyss and I. Ledoux, Chem. Rev. **94**, 77 (1994).
[4] I. Ledoux, J. Zyss, J. S. Siegel, J. Brienne, and J.-M. Lehn, Chem. Phys. Lett. **172**, 440 (1990).
[5] O. Maury and H. Le Bosec, Acc. Chem. Res. **38**, 691 (2005).
[6] G. Xing, M. Jiang, Z. Shao, and D. Xu, Chin. Phys. Lasers **14**, 302 (1987).
[7] M. Tao, M. Jiang, D. Xu, and Z. Shao, Kexue Tongbao (Foreign Lang. Ed.) **33**, 651 (1988).
[8] W. S. Wang, K. Sutter, Ch. Bosshard, Z. Pan, H. Arend, P. Gunter, G. Chapuis, and F. Nicolo, Jpn. J. Appl. Phys. **27**, 1138 (1988).
[9] H. O. Marcy, L. F. Warren, M. S. Webb, C. A. Ebbers, S. P. Velsko, G. C. Kennedy, and G. C. Catella, App. Opt. **31**, 5051 (1992).
[10] U. B. Ramabadran, D. E. Zelmon, and G. C. Kennedy, Appl. Phys. Lett. **60**, 2589 (1992).
[11] P. Kerkoc, V. Venkateramanan, S. Lochran, R. T. Bailey, F. R. Cruickshank, D. Pugh, J. N. Sherwood, R. Moseley, A. E. Goeta, C. W. Lehmann, and J. A. K. Howard, J. Appl. Phys. **80**, 6666 (1996).
[12] U. B. Ramabadran, A. L. McPherson, and D. E. Zelmon, J. Appl. Phys. **76**, 1150 (1994).
[13] V. Venkataramanan, M. R. Srinivasan, and H. L. Bhat, J. Raman Spectrosc. **25**, 805 (1994).
[14] G. D. Andretti, L. Cavalca, and A. Musatti, Acta Crystallogr. B **24**, 683 (1968).
[15] J. M. Cole, G. J. McIntyre, M. S. Lehmann, D. A. A. Myles, C. Wilkinson, and J. A. K. Howard, Acta Crystallogr. A **57**, 429 (2001).
[16] P. M. Ushasree, R. Yayavel, C. Subramanian, and P. Ramasamy, Bull. Electrochem. **14**, 407 (1998).
[17] R. Krupkova, J. Fabry, I. Cisarova, and P. Vanek, Acta Crystallogr. E **63**, m3177 (2007).
[18] N. K. Hansen and P. Coppens, Acta Crystallogr. A **34**, 909 (1978).
[19] A. P. Higginbotham, J. M. Cole, M. Blood-Forsythe, and D. D. Hickstein, J. Appl. Phys. **111**, 033512 (2012).
[20] D. Jayatilaka and D. J. Grimwood, Acta Crystallogr. A **57**, 76 (2001).
[21] S. J. Lalama and A. F. Garito, Phys. Rev. A **20**, 1179 (1979).
[22] V. Venkataramanan, F. Dhanaraj, V. K. Wadhawan, J. N. Sherwood, and H. L. Bhat, J. Cryst. Growth **154**, 92 (1995).
[23] SMART, Version 4.050 (Siemens Analytical X-ray Instruments, Inc., Madison, WI, 1995).
[24] SAINT, Version 4.050 (Siemens Analytical X-ray Instruments, Inc., Madison, WI, 1995).
[25] R. H. Blessing, Cryst. Rev. **1**, 3 (1987).
[26] R. H. Blessing, J. Appl. Cryst. **19**, 412 (1986).
[27] G. M. Sheldrick, Acta Crystallogr. A **64**, 112 (2008).
[28] H. D. Flack, Acta Crystallogr. A **39**, 876 (1983).
[29] A. Volkov, P. Macchi, L. J. Farrugia, C. Gatti, P. Mallinson, T. Richter, and T. Koritsanszky, XD2006—A computer program for multipole refinement, topological analysis of charge densities, and evaluation of intermolecular interaction energies from experimental or theoretical structure factors (2006).
[30] See Supplemental Material at http://link.aps.org/supplemental/10.1103/PhysRevB.88.184105 for details of multipolar refinement, residual electron density maps of the main molecular constituents of ZTS from the final refinement, full tabulation of the topological analysis of results pertaining to Table I, and associated charges for each ZTS atom derived from Bader and Stockholder partitioning methods.
[31] P. Coppens, B. Iversen, and F. K. Larsen, Coord. Chem. Rev. **249**, 179 (2005).
[32] T. S. Koritsanszky and P. Coppens, Chem. Rev. **101**, 1583 (2001).
[33] S. Scheins, S.-L. Zheng, J. B. Benedict, and P. Coppens, Acta Crystallogr. B **66**, 366 (2010).
[34] P. Coppens, Y. W. Yang, R. H. Blessing, W. F. Cooper, and F. K. Larsen, J. Am. Chem. Soc. **99**, 760 (1977).
[35] M. Dominiak and P. Coppens, Acta Crystallogr. A **62**, 224 (2006).
[36] E. Espinosa, E. Molins, and C. Lecomte, Phys. Rev. B **56**, 1820 (1997).
[37] F. L. Hirshfeld, Acta Crystallogr. A **32**, 239 (1976).
[38] D. Jayatilaka and D. J. Grimwood, in *Computational Science—ICCS 2003*, Lecture Notes in Computer Science Vol. 2660 (Springer, Berlin, 2003), p. 142.
[39] P. Pulay, J. Comput. Chem. **3**, 556 (1982).
[40] D. Jayatilaka, P. Munshi, M. J. Turner, J. A. K. Howard, and M. A. Spackman, Phys. Chem. Chem. Phys. **11**, 7209 (2009).

[41]D. D. Hickstein, J. M. Cole, M. J. Turner, and D. Jayatilaka, J. Chem. Phys. **139**, 064108 (2013).
[42]R. F. W. Bader, Acc. Chem. Res. **18**, 9 (1985).
[43]P. Macchi, D. M. Proserpio, and A. Sironi, J. Am. Chem. Soc. **120**, 13429 (1998).
[44]Y. A. Abramov, Acta Crystallogr. A **53**, 264 (1997).
[45]R. F. W. Bader, J. Chem. Phys. **73**, 2871 (1980).
[46]R. F. W. Bader and T. T. Nguyen-Dang, Adv. Quantum Chem. **14**, 63 (1981).
[47]R. F. W. Bader and C. Gatti, Chem. Phys. Lett. **287**, 233 (1998).
[48]G. Arfken, *Mathematical Methods for Physicists* (Academic Press, Orlando, FL, 1985).
[49]E. Monza, C. Gatti, L. L. Presti, and E. Ortoleva, J. Phys. Chem. A **115**, 12864 (2011).
[50]C. Gatti and D. Lasi, Faraday Discuss. **135**, 55 (2007).
[51]I. J. Bruno, J. C. Cole, P. R. Edgington, M. Kessler, C. F. Macrae, P. McCabe, J. Pearson, and R. Taylor, Acta Crystallogr. B **58**, 389 (2002).
[52]M. S. Schmøkel, S. Cenedese, J. Overgaard, M. R. V. Jørgensen, Y.-S. Chen, C. Gatti, D. Stalke, and B. B. Iversen, Inorg. Chem. **51**, 8607 (2012).
[53]P. P. Sun, F. F. Jian, and X. Wang, J. Chem. Crystallogr. **40**, 4 (2010).
[54]W.-Q. Zhou, L.-D. Lu, X.-J. Yang, and Y. Cao, Chem. Res. Appl. **16**, 369 (2004).
[55]W-Q. Zhou, B. Li, L. Zhu, J. Ding, Y. Zhang, L. Lu, and X. Yang, J. Mol. Struct. **690**, 145 (2004).
[56]H. Elias, D. Hess, H. Paulus, E.-G. Jager, and F. Grafe, Z. Anorg. Allg. Chem. **589**, 101 (1990).
[57]R. Carballo, J. S. Casas, E. Garcia-Martinez, G. Pereiras-Gabian, A. Sanchez, J. Sordo, and E. M. Vazquez-Lopez, Inorg. Chem. **42**, 6395 (2003).
[58]A. Bondi, J. Phys. Chem. **68**, 441 (1964).
[59]R. S. Rowland and R. Taylor, J. Phys. Chem. **100**, 7384 (1996).
[60]VISTA—A program for the analysis and display of data retrieved from the CSD, Cambridge Crystallographic Data Centre, 12 Union Road, Cambridge, United Kingdom, 1994.
[61]L. J. Farrugia and C. Evans, C. R. Chim. **8**, 1566 (2005).
[62]S. Swaminathan, B. M. Craven, M. A. Spackman, and R. F. Stewart, Acta Crystallogr. B **40**, 398 (1984).
[63]H.-P. Weber and B. M. Craven, Acta Crystallogr. B **43**, 202 (1987).
[64]F. L. Hirshfeld, Theor. Chim. Acta **44**, 129 (1977).
[65]T. C. Sarbari Girisun and S. Dhanuskodi, Cryst. Res. Technol. **44**, 1297 (2009).
[66]K. Clays and A. Persoons, Phys. Rev. Lett. **66**, 2980 (1991).
[67]B. F. Levine and C. G. Bethea, Appl. Phys. Lett. **24**, 445 (1974).
[68]R. Shi and A. Garito, in *Characterization Techniques and Tabulations for Organic Nonlinear Optical Materials* (Marcel Dekker, New York, 1998), pp. 1–36.
[69]D. A. Kleinman, Phys. Rev. **126**, 1977 (1962).
[70]See, for example, C. A. Dailey, B. J. Burke, and G. J. Simpson, Chem. Phys. Lett. **390**, 8 (2004).
[71]J. M. Cole, R. C. B. Copley, G. J. McIntyre, J. A. K. Howard, M. Szablewski, and G. H. Cross, Phys. Rev. B **65**, 125107 (2002).
[72]J. M. Cole, A. E. Goeta, J. A. K. Howard, and G. J. McIntyre, Acta Crystallogr. B **58**, 690 (2002).
[73]M. A. Spackman, Chem. Rev. **92**, 1769 (1992).
[74]T. C. Lin, J. M. Cole, A. P. Higginbotham, A. J. Edwards, R. O. Piltz, J. P-Moreno, J.-Y. Seo, J.-S. Lee, K. Clays, and O.-P. Kwon, J. Phys. Chem. C **117**, 9416 (2013).
[75]J. M. Cole, J. A. K. Howard, and G. J. McIntyre, Acta Crystallogr. B **57**, 410 (2001).